ADVANCED ENERGY MATERIALS
www.advenergymat.de

Large-Area Preparation of Crack-Free Crystalline Microporous Conductive Membrane to Upgrade High Energy Lithium–Sulfur Batteries

Ying Zang, Fei Pei, Jiahong Huang, Zhihua Fu, Gang Xu, and Xiaoliang Fang**

Dedicated to Professor Jin-shun Huang on the occasion of his 80th birthday

Lithium–sulfur (Li–S) batteries are appealing candidates for next-generation high-energy rechargeable batteries, but practical applications are still limited by poor cyclic life, which is caused by severe polysulfide shuttling in high-sulfur-loading batteries. Herein, a facile route is presented to fabricate high-performance Li–S batteries using a crystalline microporous membrane, which is prepared using a conductive metal–organic framework (MOF) material. With ordered microporous structure, large specific surface area, good sulphiphilicity, and excellent conductivity, the MOF membrane is grown in situ on the commercial separator and is an ideal light-weight barrier (0.066 mg cm^{-2}) for suppressing the polysulfide shuttling, which can significantly promote the capacities, rate capabilities, and cycling stabilities of Li–S batteries. Taking the advantage of this functional separator, the high-sulfur-loading Li–S battery (8.0 mg cm^{-2} and 70 wt% of sulfur in cathode) delivers a high area capacity of 7.24 mAh cm^{-2} after 200 cycles, thus providing a promising path toward advanced Li–S batteries.

Lithium–sulfur (Li–S) batteries are a promising technology to meet the demand of low-cost and high-density energy storage.[1–4] Benefited from the progress in sulfur-hosting materials, the specific capacities and cycling stabilities of Li–S cathodes have obviously improved.[5–13] Unfortunately, the fast capacity degradation of high-sulfur-loading cathodes, caused by the shuttling of polysulfide intermediates (Li_2S_n; $4 \le n \le 8$), is still a bottleneck, which limits the development of high-energy-density Li–S batteries.[14,15] Recently, intercepting the diffusing polysulfides by inserting a barrier layer between the cathode and the separator brings new vitality into Li–S batteries.[16–21] An ideal barrier layer should be: i) a continuous, crack-free sieving membrane with uniform pore structures to transfer Li^+ while blocking polysulfides; ii) light weight and thin enough to avoid reducing the overall sulfur content of batteries; iii) highly conductive to serve as an expanded current collector to decrease the resistance of batteries and improve the sulfur utilization.[16–21] It is worth mentioning that simultaneously fulfilling all these requirements is challenging. All reported barrier layers provided channels with irregular size distribution, which deteriorate the sieving efficiency between Li^+ and polysulfides. A big progress regarding the preparation of a large-area, crack-free, microporous membrane is extremely desired to truly validate the barrier concept in Li–S batteries. In this work, it is demonstrated that several unique features of conductive metal–organic frameworks (MOFs) make it fully feasible to fabricate such an ideal barrier layer for high-performance Li–S batteries.

With high porosity, uniform pore size, tunable pore parameters, and high affinity to guest molecules, MOFs have shown great potential in various applications, such as separation, gas storage, catalysis, sensing, and energy conversion and storage.[22–28] Although their excellent molecular sieving ability and high binding energies to polysulfides make MOFs the fascinating barrier materials in Li–S batteries,[29] most of the efforts have focused on the design of Li–S cathodes derived from MOF particles.[30–33] In order to construct an ideal barrier layer, MOFs are required to consist of continuous and crack-free membranes to exert their advantages in molecular sieving. Unfortunately, it remains challenging to fabricate large-area high-quality MOF membranes using traditional methods for fabricating organic polymer membranes, as they are often at least micrometer-sized crystallites and insoluble in solvents.[34] In order to prepare MOF membranes, some elaborate methods, such as physically or chemically combining MOF particles with organic polymers, growing MOFs within porous supports, or filtering MOF particles together with other materials (for example, graphene oxide),

Y. Zang, J. H. Huang, Z. H. Fu, Prof. G. Xu
State Key Laboratory of Structural Chemistry
Fujian Institute of Research on the Structure of Matter
Chinese Academy of Sciences
Fuzhou, Fujian 350002, China
E-mail: gxu@fjirsm.ac.cn
Y. Zang
College of Chemistry and Molecular Engineering
Zhengzhou University
Zhengzhou 450001, China
F. Pei, Dr. X. L. Fang
Pen-Tung Sah Institute of Micro-Nano Science and Technology
Xiamen University
Xiamen, Fujian 361005, China
E-mail: x.l.fang@xmu.edu.cn
Prof. G. Xu
University of Chinese Academy of Sciences
Chinese Academy of Sciences
Beijing 100039, China
The ORCID identification number(s) for the author(s) of this article can be found under https://doi.org/10.1002/aenm.201802052.

DOI: 10.1002/aenm.201802052

have been developed in recent years.[35] Despite considerable progress, poor compatibility between MOFs and depositing substrates often leads to the presence of cracks and intercrystallite voids in most hybrid MOF membranes, thus lacking sufficient homogeneity for molecular sieving applications. Direct synthesis of continuous and phase pure MOF membranes is expected as an effective alternative to solve these problems. However, the preparation of continuous large-area MOF membranes, especially with controlled thickness, has not been achieved yet. Moreover, MOF materials are usually nonconductive, making it extremely difficult to satisfy the requirement of barrier layer to be electronically conductive. Therefore, the tunable preparation of large-area phase-pure MOF membranes with small thickness and high conductivity is not only of great significance in both fundamental and application of MOF materials, but will also help in creating new Li–S batteries.

In this work, the preparation of a large-area, crack-free, and microporous membrane has been reported using a conductive MOF, $Ni_3(HITP)_2$ (HITP = 2,3,6,7,10,11-hexaiminotriphenylene). It has been demonstrated for the first time that crystalline microporous membrane is a favorable barrier layer for the construction of high-performance Li–S batteries. With a low mass loading (≈0.066 mg cm^{-2}), the continuous $Ni_3(HITP)_2$ membrane can be directly prepared on a commercial separator using a novel interface-induced growth process. Benefitting from its uniform 1D microporous channels, favorable absorption capacity for polysulfides, and high conductivity, the $Ni_3(HITP)_2$ membrane can significantly improve the rate capability (589 mAh g^{-1} at 5 C) and cyclic performance (716 mAh g^{-1} after 500 cycles at 1 C) of the slurry-coated S/carbon black cathode with the sulfur content of 64 wt% and area sulfur loading of 3.5 mg cm^{-2}. Furthermore, by using the $Ni_3(HITP)_2$ membrane, the self-supporting S/carbon nanotubes cathode with the sulfur content of 70 wt% and high area sulfur loading of 8.0 mg cm^{-2} deliver a high area capacity of 7.24 mAh cm^{-2} after 200 cycles at 0.5 C, which is among the best sulfur utilization and cyclic stability in Li–S batteries having similar sulfur loading.

The assembly of square-planar coordinated metal ions (e.g., Ni^{2+} and Cu^{2+}) with π-conjugated ligands (e.g., hexahydroxy-, hexaimino-, and hexathio-triphenylene) spawns a recent class of 2D layered MOFs.[36–41] Compared with the traditional MOFs, this category of MOFs is very distinctive due to their high electronic conductivities and unique structural features. Considering $Ni_3(HITP)_2$ as an example (**Figure 1**), it is found that $Ni_3(HITP)_2$ is one of the most conductive MOFs reported so far with the conductivity of 4000 S m^{-1}, which is four times higher than those of the activated carbon and holey graphite.[36,37] Structurally, the coordination of Ni^{2+} centers and tritopic HITP ligands forms a 2D layer structure with hexagonal pores in the *ab* plane. The packing of these 2D layers through strong π–π interaction makes up a honey-comb structure with uniform 1D channels along the *c* axis. Notably, the walls of these channels are rich in polar sites (i.e., the electronegative N elements), which are favorable for binding the polar polysulfides.[3] Previous works have reported that a freestanding $Ni_3(HITP)_2$ membrane can spontaneously form at the liquid–air interface of the mixed aqueous solution of nickel chloride and HITP (Figure S1, Supporting Information).[36,40] These advantages of $Ni_3(HITP)_2$ inspired its use as a polysulfide barrier layer. However, the liquid–air interface derived $Ni_3(HITP)_2$ membrane is fragile. It is difficult to take out an undamaged $Ni_3(HITP)_2$ membrane from the liquid–air interface, even by using a solid substrate to transfer it (Figure S1, Supporting Information). In this work, it is found that large area $Ni_3(HITP)_2$ membrane could be

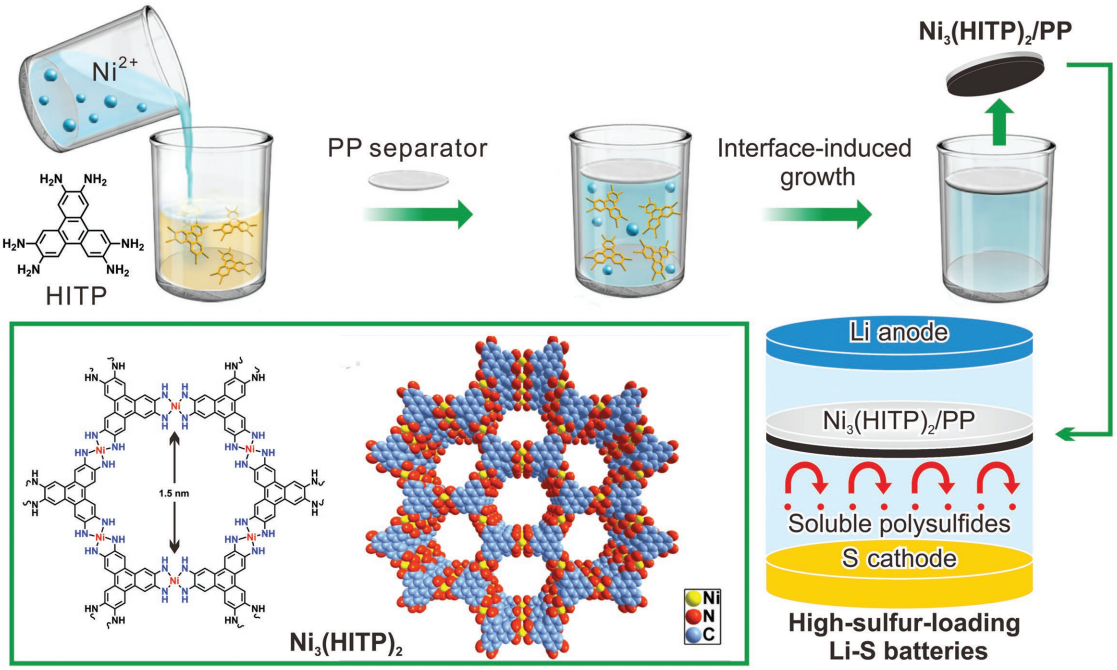

Figure 1. Schematic illustration of the interface-induced growth of the conductive $Ni_3(HITP)_2$ modified separator for the application in Li–S batteries. 2D layered structure gives $Ni_3(HITP)_2$ a uniform 1D pore channels, and the $Ni_3(HITP)_2$ membrane (black color) grown directly on the surface of the commercial polypropylene separator can be used as a barrier for the suppression of the polysulfide shuttling.

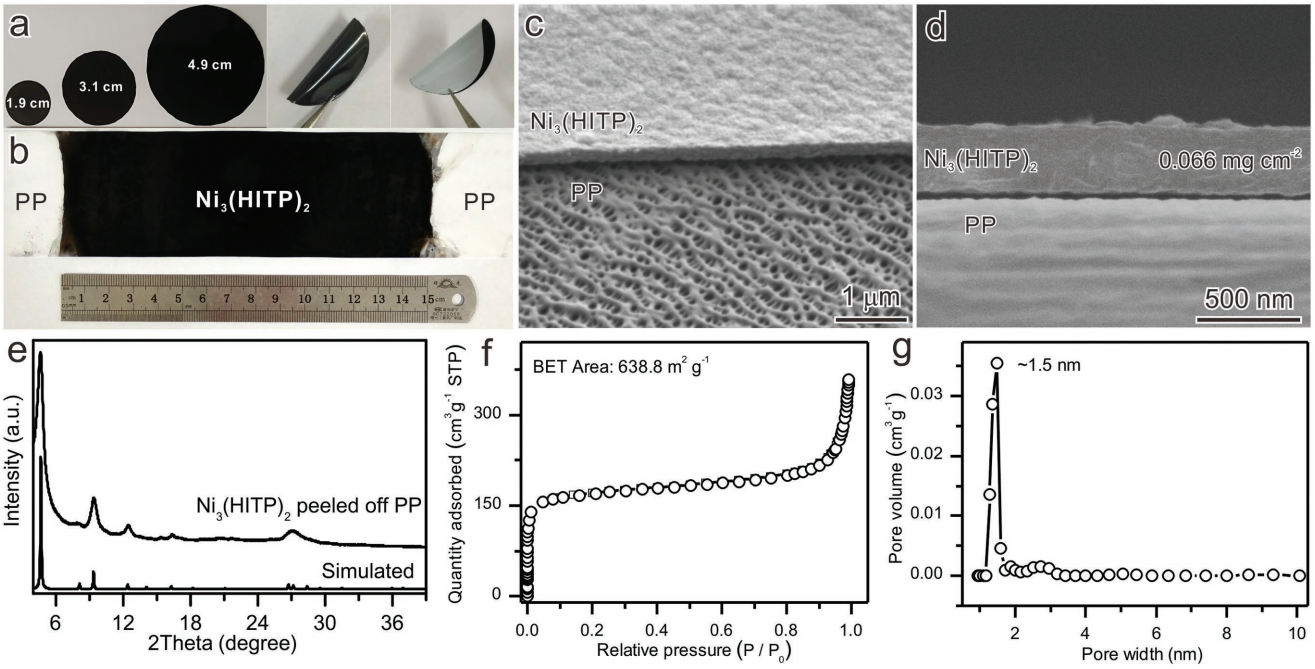

Figure 2. Characteristics of the $Ni_3(HITP)_2$ modified separator. a) Photographs of the $Ni_3(HITP)_2$ modified separators with different sizes and the flexibility of the $Ni_3(HITP)_2$ modified separator. b) Photograph of the large area $Ni_3(HITP)_2$ modified separators. c,d) Cross-section SEM images of low-mass loading $Ni_3(HITP)_2$ membrane (0.066 mg cm^{-2}) on the PP separator. e) XRD pattern, f) N_2 sorption isotherm, and g) pore-size distribution of $Ni_3(HITP)_2$.

fabricated at a liquid–solid interface, created by floating a substrate on the reaction solution (see the Experimental Section for more details). The light-weight and hydrophobic commercial polypropylene (PP) separator (Celgard 2400) is preferred as an available substrate and the resulting $Ni_3(HITP)_2$/PP membrane can be directly used in Li–S batteries (Figure 1).

As shown in **Figure 2**, the high-quality $Ni_3(HITP)_2$ membranes (≈0.066 mg cm^{-2}; ≈340 nm) could be limitedly grown on one side of PP separator by replacing the water–air interface with the proposed water–solid interface. The as-prepared $Ni_3(HITP)_2$/PP separator is a Janus membrane with conductive $Ni_3(HITP)_2$ side and insulating PP side. Such a Janus structure gives rise to a multifunctional $Ni_3(HITP)_2$/PP separator. The conductive side (i.e., $Ni_3(HITP)_2$ layer) can work as both a barrier layer and an expanded current collector to suppress the polysulfide shuttling and simultaneously increase the utilization of sulfur. The insulating side (i.e., PP layer) helps avoid short circuiting between cathode and anode. More importantly, the proposed interface-induced growth method has application potential in the synthesis of large-area MOF membrane. Simply by increasing the lateral sizes of the commercial PP separator, the sizes of $Ni_3(HITP)_2$ membrane can be easily scaled up (Figure 2a). The $Ni_3(HITP)_2$ membrane with the dimensions of 15.0 cm × 5.2 cm was successfully grown on the commercial PP separator, which is much larger than most MOF membranes reported so far (Figure 2b). The mechanical properties of $Ni_3(HITP)_2$ membrane improved tremendously after receiving support from PP separator, as demonstrated by the folding test (Figure 2a). Owing to excellent adhesion of PP to $Ni_3(HITP)_2$, the $Ni_3(HITP)_2$ membrane is not easy to peel off. The scanning electron microscope (SEM) image of $Ni_3(HITP)_2$/PP, sliced using a sharp knife, clearly reveals that the pristine PP separator possesses a highly porous structure with the pore sizes ranging from several tens to hundreds of nanometers (Figure 2c). Meanwhile, a dense layer of microporous $Ni_3(HITP)_2$ completely covers the surface of PP separator (Figure 2d). The typical cross-sectional SEM image and atomic force microscope (AFM) image further indicate that the thickness of $Ni_3(HITP)_2$ membrane is only about 340 nm, which is far thinner than most of the barrier layers reported previously (Figure 2c; Figure S2 and Table S1, Supporting Information). Moreover, the thickness of $Ni_3(HITP)_2$ membrane can be fine-tuned within the range of 90–970 nm by controlling the reaction time (Figures S3 and S4, Supporting Information). A significant advantage of such a crack-free structure is that the conductivity of $Ni_3(HITP)_2$ membrane (3720 S m^{-1}) is significantly higher than that of the powder-compressed pellets (50 S m^{-1}) due to less grain boundary. The X-ray diffraction (XRD) pattern (Figure 2e) of $Ni_3(HITP)_2$ powder scratched from $Ni_3(HITP)_2$/PP membrane agrees well with that simulated using the crystal structure of $Ni_3(HITP)_2$. The type I N_2 adsorption–desorption isotherm further confirms the microporous feature of $Ni_3(HITP)_2$ membrane, while the specific surface area of $Ni_3(HITP)_2$ membrane is found to be 638.8 m^2 g^{-1} (Figure 2f). According to the pore size distribution curve, the $Ni_3(HITP)_2$ membrane has a very narrow pore size distribution, which is centered at 1.5 nm and is consistent with the value deduced from its crystal structure (Figure 2g). Compared with the marcoporous structure of PP separator, the uniform micropores of $Ni_3(HITP)_2$ membrane could reduce the permeation of polysulfides more effectively.

In order to improve the polysulfide-entrapping properties of the barrier modified separators, two strategies are commonly

used. One is to reduce the size of the channels in the barrier layers, so that the diffusion resistance of the polysulfides is increased, while the other is to increase the interaction between the barrier materials and polysulfides to increase the polysulfide-capturing abilities of the barrier layers.[16–21] Therefore, the ability of $Ni_3(HITP)_2$ for adsorbing polysulfides was evaluated using conventional barrier materials (such as graphene, carbon nanotubes (CNT), and carbon black (CB)) and typical MOF particles (such as HKUST-1 and ZIF-8) as the reference adsorbents. For comparison, the same weights (100 mg) of the adsorbents were added into polysulfide (Li_2S_6) tetrahydrofuran solutions (5.0 mL; 4×10^{-3} M). The orange-colored Li_2S_6 tetrahydrofuran solution becomes colorless only when $Ni_3(HITP)_2$ is added (**Figure 3**a). Based on the corresponding UV–vis absorption spectra, the saturated adsorption capacities of $Ni_3(HITP)_2$, CB, CNT, graphene, HKUST-1, and ZIF-8 for Li_2S_6 are found to be 0.183, 0.097, 0.086, 0.076, 0.041, and 0.032 mmol g^{-1}, respectively. This result indicates that the polysulfide-capturing ability of $Ni_3(HITP)_2$ is far superior to other five reference materials (Figure 3b,c). Although it has been shown that MOFs are a class of sulfur host materials with higher ability of chemically bond with polysulfides compared with the pristine carbon materials, HKUST-1 and ZIF-8 showed lower adsorption capabilities due to their smaller channel apertures (0.9 nm for HKUST-1 and 0.34 nm for ZIF-8), which actually result in a limited available interface for binding polysulfides. Since the void space among the barrier materials is inevitable and the channels created by the packing of the barrier materials always exist with relatively large size distribution, the size selectivities of the reported barrier layers are still not good enough to completely intercept polysulfide diffusion.[42–44] This situation will become much worse in high-sulfur-loading batteries. Therefore, the uniform 1D channels with suitable aperture size and large amount of accessible binding sites of $Ni_3(HITP)_2$ are very important in promoting the polysulfide-entrapping property of $Ni_3(HITP)_2$/PP separator.

The permeability of polysulfides through $Ni_3(HITP)_2$ membrane was further investigated, as shown in Figure 3d,e. The deep red Li_2S_6 tetrahydrofuran solution and pure tetrahydrofuran were separated using $Ni_3(HITP)_2$/PP separator in a H-type glass cell. The control experiment was performed by keeping other conditions the same and using PP separator instead of $Ni_3(HITP)_2$/PP separator. A visible migration of polysulfides through PP separator to pure colorless tetrahydrofuran side was detected only after 5 min (Figure 3d). By a sharp contrast, no polysulfide diffusion was observed until 36 h when $Ni_3(HITP)_2$/PP separator was used (Figure 3e). It is noteworthy that the weight and thickness of $Ni_3(HITP)_2$ membrane on the PP separator are significantly lower than most of the barrier layers reported previously, indicating its excellent performance in suppressing polysulfides shuttling.[16–18] The use of large quantities of barrier materials (usually >0.3 mg cm^{-2}) is a common problem faced by most barrier layers, which undoubtedly reduces the sulfur contents of Li–S batteries (Table S1, Supporting Information). Therefore, the permeation experiment suggests that the $Ni_3(HITP)_2$ membrane would be very promising for use as a light-weight barrie against the "shuttle effect."

In order to evaluate the performance of $Ni_3(HITP)_2$ membrane in Li–S batteries, the S/C cathode was constructed using commercial CB as the sulfur host material. After the melt-diffusion process, the sulfur content of S/CB composites was as high as 80 wt% (Figure S5, Supporting Information), while the corresponding S/CB cathode had the sulfur content of 64 wt% and sulfur loading of 3.5 mg cm^{-2}, which was obtained using conventional slurry-coating method. The sulfur content of cathode with extra barrier layers was about 63.2 wt%, indicating

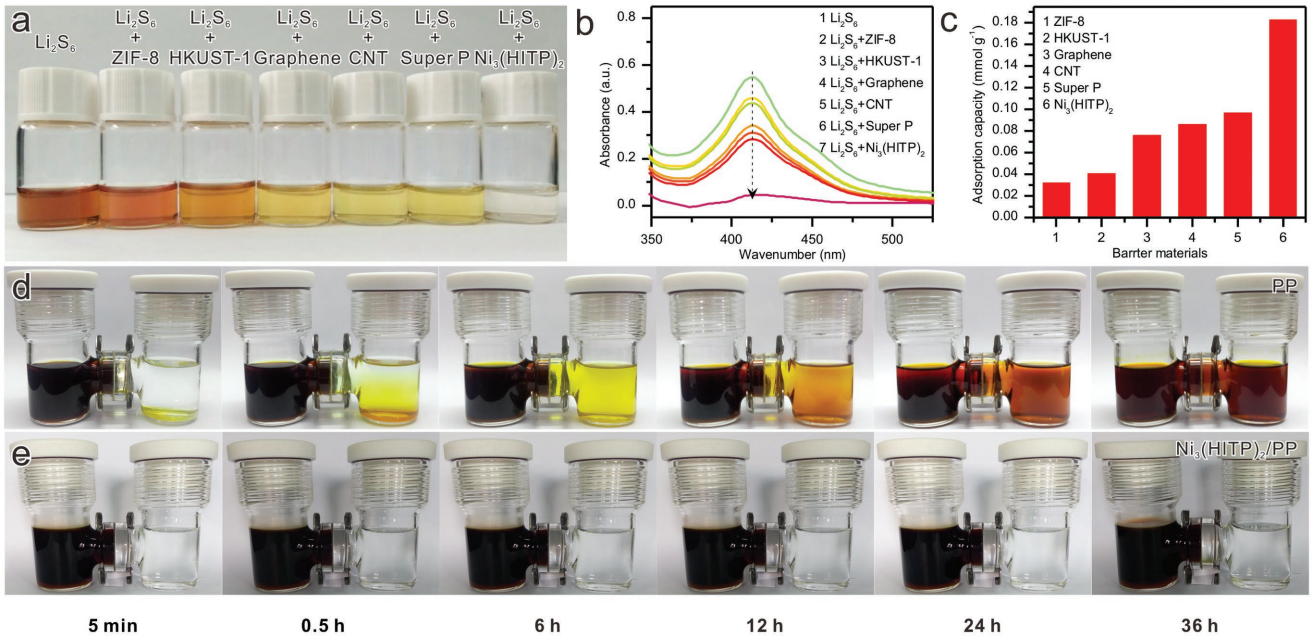

Figure 3. Polysulfide capturing tests. a) Photograph and b) UV–Vis absorption spectra for the Li_2S_6 solution treated with different barrier materials. c) Comparison of the absorption capacities of different barrier materials for Li_2S_6. d,e) Polysulfide permeation tests for the PP separator and $Ni_3(HITP)_2$ modified separator, respectively.

that the $Ni_3(HITP)_2$ membrane has almost no influence on the sulfur content of the batteries. Notably, for higher energy density, the sulfur loading of S/CB cathode is about 2–3 times higher than those of the conventional sulfur composite cathodes (Table S1, Supporting Information). Due to higher sulfur content together with higher sulfur loading, this S/CB cathode has to face a more serious problem of polysulfide shuttling, thus providing an ideal system to investigate the performance of $Ni_3(HITP)_2$ barrier layer. For comparison, five S/CB-based Li–S coin cells were assembled by employing PP separator or PP separators with different barrier layers ($Ni_3(HITP)_2$, graphene, CNT, and ZIF-8), and were denoted as PP, $Ni_3(HITP)_2$/PP, G/PP, CNT/PP, ZIF-8/PP, respectively (Figure S6, Supporting Information). Both graphene and CNT barrier layers on PP separators were obtained using a facile vacuum filtration deposition process. ZIF-8 barrier layer on PP separator was fabricated according to the same procedure as used for $Ni_3(HITP)_2$ modified separator (see the Experimental Section for details). For comparison, the weights of all barrier layers were precisely controlled at 0.066 mg cm^{-2}.

The galvanostatic charge/discharge behaviors of Li–S coin cells were first measured within a potential window of 1.7–2.8 V against Li^+/Li^0. It is worth mentioning that the $Ni_3(HITP)_2$ membrane is very stable within this potential window (Figure S7, Supporting Information). As shown in **Figure 4**a and Figures S8–S11 (Supporting Information), two voltage plateaus located around 2.3 and 2.1 V in the discharge curves correspond to the typical multistep reduction process from solid S_8 to soluble polysulfides Li_2S_{4-8}, and then, to insoluble products Li_2S_2/Li_2S. Based on the discharge curves at 0.2 C (1 C = 1675 mA g^{-1}), the initial discharge capacity of $Ni_3(HITP)_2$/PP (1244 mAh g^{-1}) is calculated using the weight of sulfur and is found to be higher than those of G/PP (1146 mAh g^{-1}), CNT/PP (1082 mAh g^{-1}), ZIF-8/PP (945 mAh g^{-1}), and PP (889 mAh g^{-1}), indicating higher sulfur utilization endowed by the $Ni_3(HITP)_2$ barrier layer. The higher capacity of $Ni_3(HITP)_2$/PP can be attributed to favorable conductivity of $Ni_3(HITP)_2$ barrier, which resulted in a lower internal resistance compared to other four cells (Figure S12, Supporting Information). Meanwhile, the electrical impedance spectroscopy measurements

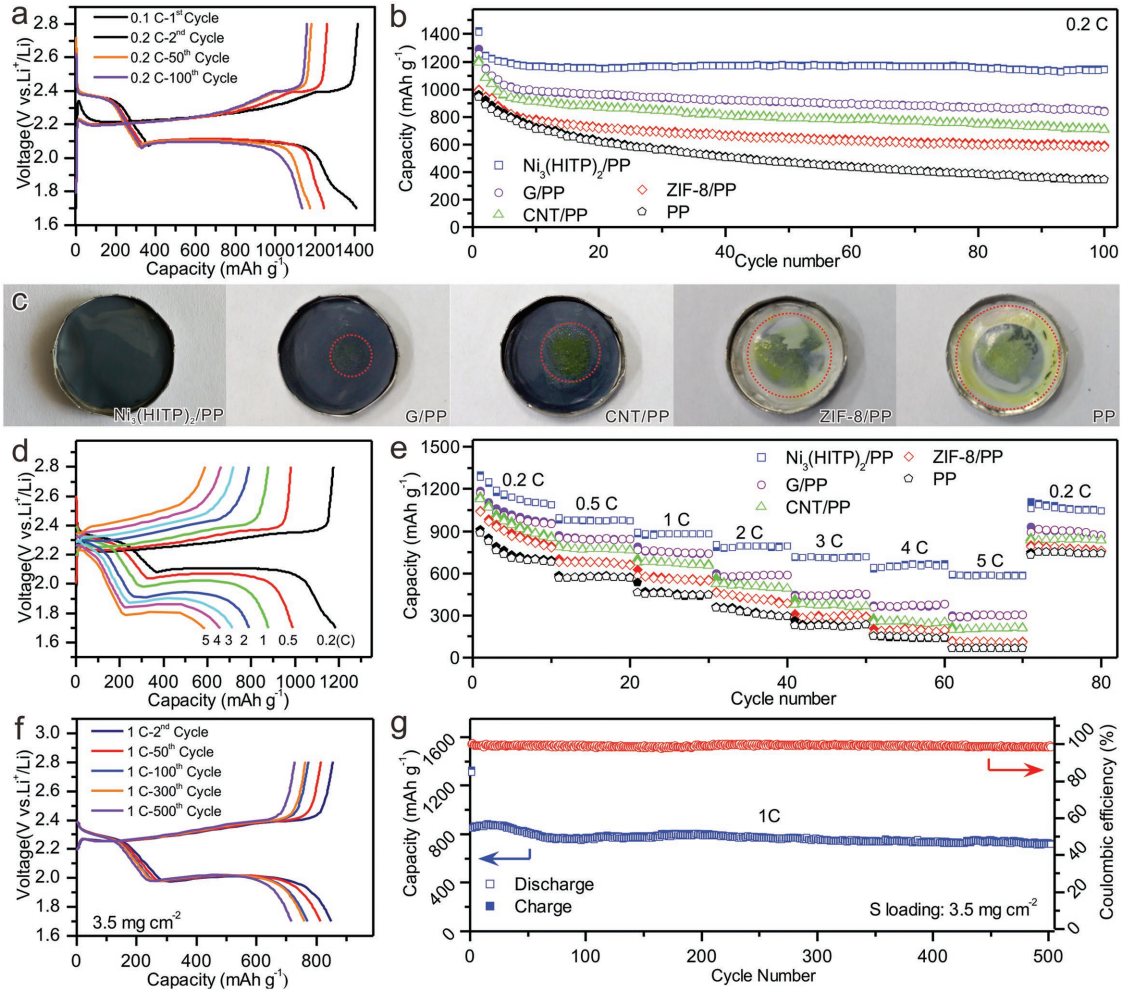

Figure 4. Electrochemical performance of the slurry-coated cathodes decorated with different separators. a) Charge/discharge curves of $Ni_3(HITP)_2$/PP at 0.2 C. b) Cycling performance of $Ni_3(HITP)_2$/PP, G/PP, CNT/PP, ZIF-8/PP, and PP at 0.2 C. c) Photos of the separators after 100 cycles at 0.2 C. d) Charge/discharge curves of $Ni_3(HITP)_2$/PP at different rates. e) Rate capabilities of $Ni_3(HITP)_2$/PP, G/PP, CNT/PP, ZIF-8/PP, and PP. f) Charge/discharge curves and g) cycling performance of $Ni_3(HITP)_2$/PP at 1 C.

indicate that the $Ni_3(HITP)_2$ membrane has no negative impact on the transport of Li^+ (Figure S13, Supporting Information). After 100 cycles, the discharge capacities of 1139, 838, 703, 581, and 342 mAh g^{-1} were maintained for $Ni_3(HITP)_2$/PP, G/PP, CNT/PP, ZIF-8/PP, and PP, respectively, and accounted for 92%, 73%, 65%, 61%, and 38% of their initial capacities, respectively (Figure 4b). Not surprisingly, the amount of dissolved polysulfides, adhering to the surface of separators after the cycling tests, increased in the following order: PP > ZIF-8/PP > CNT/PP > G/PP > $Ni_3(HITP)_2$/PP (Figure 4c). These results reveal that: 1) the introduction of barrier layers can dramatically improve the sulfur utilization and cycling stability of S/CB cathode compared with the commercial PP separator; 2) the trapping ability of $Ni_3(HITP)_2$ barrier for polysulfides is significantly superior than those of the other four barriers.

In order to further reveal the advantages of $Ni_3(HITP)_2$ barrier, the five coin cells were analyzed for galvanostatic discharge/charge at different current rates. As shown in Figure 4d,e and Figures S14–S17 (Supporting Information), the discharge capacities of $Ni_3(HITP)_2$/PP at 0.2, 0.5, 1, 2, 3, 4, and 5 C were 1186, 990, 879, 790, 716, 659, and 589 mAh g^{-1}, respectively. When the current density is switched back to 0.2 C, a discharge capacity of 1090 mAh g^{-1} was recovered, revealing good stability of $Ni_3(HITP)_2$/PP after discharging/charging at high current rates. More importantly, at the current rate of 5 C, the capacities of $Ni_3(HITP)_2$/PP were 1.9, 2.9, 5.1, and 9.3 times higher than those of G/PP (304 mAh g^{-1}), CNT/PP (205 mAh g^{-1}), ZIF-8/PP (116 mAh g^{-1}), and PP (63 mAh g^{-1}), respectively, demonstrating the enhanced performance of $Ni_3(HITP)_2$/PP. Compared with $Ni_3(HITP)_2$/PP, the lower sulfur utilizations of other four coin cells at high current rates are mainly caused by their increased internal resistances during the cycles at low current rates (Figure S18, Supporting Information). Based on its favorable capacity and rate performance, the long-term cycling stability of $Ni_3(HITP)_2$/PP was further evaluated at a high current rate of 1 C (Figure 4f,g). After one activation cycle at 0.1 C, $Ni_3(HITP)_2$/PP delivered an initial discharge capacity of 851 mAh g^{-1} at 1 C. During the cycling process, the Coulombic efficiency (CE) of $Ni_3(HITP)_2$/PP always remained around 99%. After 500 cycles at 1 C, the final capacity of $Ni_3(HITP)_2$/PP was as high as 716 mAh g^{-1}, which corresponded to a high capacity retention of 84.1% and a low average capacity decay of 0.032% per cycle. Importantly, the cycling stability of $Ni_3(HITP)_2$/PP based Li–S battery is superior to most of the Li–S batteries even when expensive host materials or high-weight barrier layers are used, thus highlighting the advantages of $Ni_3(HITP)_2$ barrier (Figure S19 and Tables S1 and S2, Supporting Information).[6–12]

It is well known that the high theoretical energy density is one of the most important advantages of Li–S batteries. Unfortunately, most of the reported Li–S batteries are usually constructed using low-sulfur-loading cathodes.[14] The capacity densities of the reported Li–S batteries are usually lower than the state-of-the-art Li-ion batteries (≈4 mAh cm^{-2}). In order to surpass Li-ion batteries, employing a self-supporting cathode without the use of additives, such as the conductive agents, binders, and metallic current collector, has recently emerged as an effective route to obtain high-sulfur-loading cathodes with increased areal capacities.[45–48] However, simply increasing the sulfur mass and areal loading of cathodes always results in low sulfur utilization and poor cyclic stability of high-energy-density Li–S batteries.[3,45–48]

In order to reveal the application potential of $Ni_3(HITP)_2$ barrier in high-energy-density Li–S batteries, commercial CNT was used for the fabrication of high-sulfur-loading cathodes. As shown in **Figure 5**a, the self-supporting S/CNT cathode with the areal sulfur loading as high as 8 mg cm^{-2} was prepared using vacuum filtration of CNT aqueous dispersion and subsequent sulfur impregnation into as-obtained CNT paper using a melt-diffusion approach. The thermogravimetric analysis (TGA) reveals that the sulfur content of S/CNT cathode is as high as 70.0 wt% (Figure 5b). The SEM images further indicate that the high amount of sulfur is beyond the binding surface provided by CNT, whereas many sulfur particles are piled in the voids among S/CNT composites (Figure 5c,d). For comparison, the $Ni_3(HITP)_2$/PP and PP were separately used as the separators for S/CNT cathode. The corresponding coin cells, S/CNT-$Ni_3(HITP)_2$/PP and S/CNT-PP, were tested at 0.5 C (Figure 5e,f). After 2 activation cycles at 0.05 C, the initial capacities of S/CNT-$Ni_3(HITP)_2$/PP and S/CNT-PP at 0.5 C were 1055 mAh g^{-1} (8.44 mAh cm^{-2}) and 920 mAh g^{-1} (7.36 mAh cm^{-2}), respectively, indicating that the $Ni_3(HITP)_2$ barrier can help improve the sulfur utilization of high-sulfur-loading cathodes. After 200 cycles, the reversible capacities of S/CNT-$Ni_3(HITP)_2$/PP were found to be 905 mAh g^{-1} (7.24 mAh cm^{-2}), representing a capacity retention of 86%. During the cycling test, the areal capacity of S/CNT-$Ni_3(HITP)_2$/PP was consistently higher than that of the state-of-the-art Li-ion batteries (Figure 5g). By contrast, S/CNT-PP showed a fast capacity loss during the cycling test, and delivered a low capacity of 271 mAh g^{-1} (2.17 mAh cm^{-2}) with the retention of only 29% after 200 cycles. Although the capacity and cycling stability of S/CNT-$Ni_3(HITP)_2$/PP are already superior to many other high-sulfur-loading Li–S batteries (Figure S20 and Table S3, Supporting Information), the performance of Li–S batteries based on $Ni_3(HITP)_2$/PP separator could be further enhanced by using structure-optimized cathodes.[49–51] Therefore, using MOF membrane as a barrier layer separator would be a convenient route to create high-energy-density Li–S batteries.

In summary, the large-area high-quality microporous membranes were successfully designed and prepared using a highly conductive MOF, $Ni_3(HITP)_2$, to truly demonstrate the polysulfide barrier concept in Li–S batteries. The liquid–solid interface method, proposed and developed in this work, provides a new route to prepare crack-free and phase pure MOF membranes having very large area (over 75 cm^2) and controlled thickness (90–970 nm). Highly ordered micropores, excellent polysulfide-entrapping ability, good conductivity (3720 S m^{-1}), and low density make $Ni_3(HITP)_2$ membrane an ideal polysulfide barrier to optimize high-sulfur-loading Li–S batteries constructed using commercial host materials. As results, the capacities, rate capabilities, and especially the cyclic stabilities of the batteries were significantly enhanced, where a low average capacity decay of 0.032% per cycle was achieved. Even for the cathode with sulfur loading of up to 8.0 mg cm^{-2} and 70 wt%, the low-mass loading $Ni_3(HITP)_2$ barrier (≈0.066 mg cm^{-2}) can help provide a high areal capacity of up to 8.44 mAh cm^{-2} and a high capacity retention of 86% after 200 cycles. Given the versatile structures, chemically modifiable functional groups on organic linkers, and flexible modulation of the properties of MOFs, it is believed that

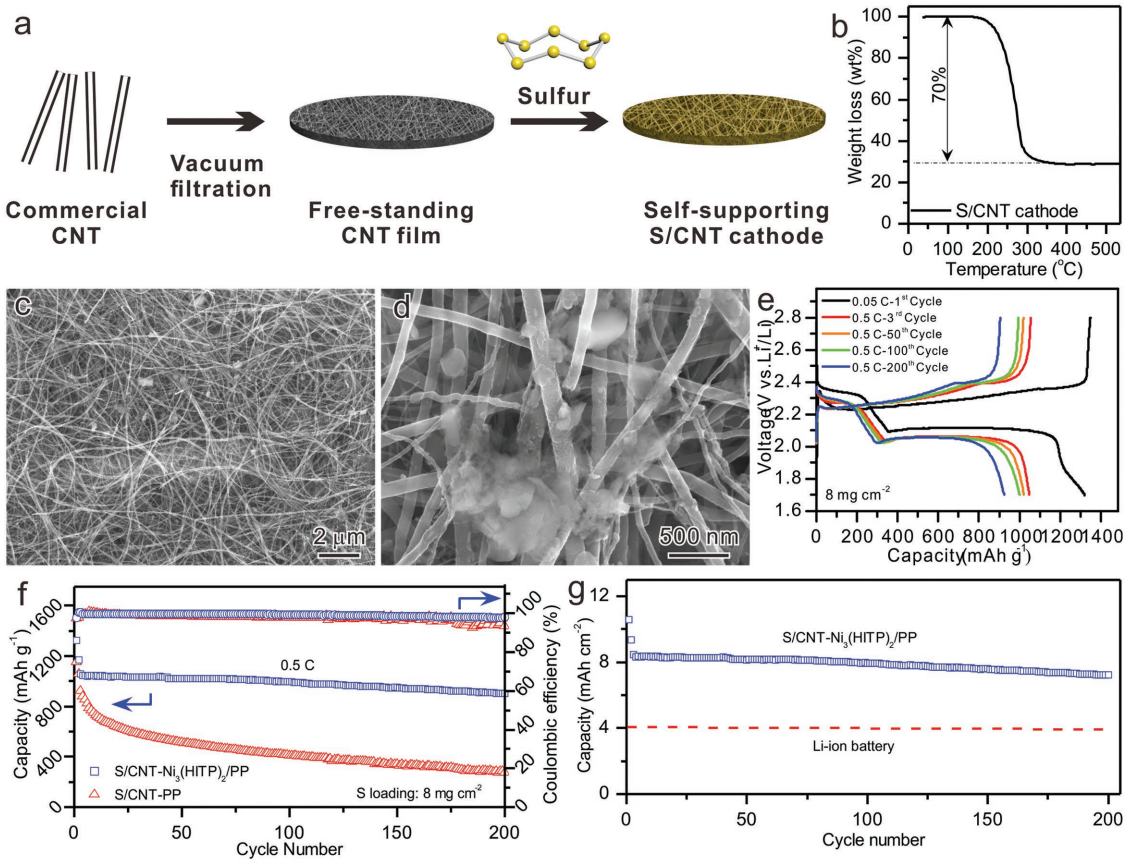

Figure 5. Electrochemical performance of the self-supporting cathode decorated with the $Ni_3(HITP)_2$/PP separator. a) Schematic illustration for the preparation of the S/CNT cathode. b) TGA curve and c,d) SEM images of the S/CNT cathodes. e) Charge/discharge curves of S/CNT-$Ni_3(HITP)_2$/PP at 0.5 C. f) Cycling performance of S/CNT-PP and S/CNT-$Ni_3(HITP)_2$/PP at 0.5 C. g) Areal capacity of S/CNT-$Ni_3(HITP)_2$/PP at 0.5 C. The weight of the $Ni_3(HITP)_2$ barrier layer is 0.66 mg cm^{-2}. The capacities in (f) and (g) were calculated based on the discharge curves.

the concept of high-performance and low-mass loading MOF barriers will push forward the future development of Li–S batteries.

Experimental Section

Chemicals: All chemicals were purchased through commercial suppliers and used without further purification. Water used in this work was purified using the Milli-Q purification system. Nickel chloride hexahydrate, sublimed sulfur, zinc nitrate hexahydrate, 2-methylimidazole, absolute ethanol, and ammonium hydroxide were purchased from Sinopharm Chemical Reagent Co., Ltd., China. Commercial CNT powder was obtained from Wuhan ATMK Super EnerG Technologies Inc., China. Furthermore, 2,3,6,7,10,11-hexaaminotriphenylene hexahydrochloride was prepared according to the procedure available in previous works.[36,52]

Preparation of $Ni_3(HITP)_2$ or ZIF-8 Membrane Coated Separator: 10 mL of nickel chloride aqueous solution (3.8×10^{-3} M) was mixed with 10 mL of 2,3,6,7,10,11-hexaaminotriphenylene aqueous solution (5.6×10^{-3} M) with continuous stirring at 65 °C under air atmosphere. Then, ammonium hydroxide (300 μL) was added to the solution. A tailored Celgard 2400 separator was placed on the surface of the solution. After reaction at 65 °C for 2 h, the $Ni_3(HITP)_2$ membrane coated polypropylene separator was washed with ethanol and ultrapure water, and then, dried under vacuum at 30 °C. Later, the zinc nitrate aqueous solution, 2-methylimidazolee aqueous solution, and Celgard 2400 separator were used to fabricate the ZIF-8 coated separator according to the same procedure.

Preparation of Graphene or CNT Coated Separator: Typically, 10 mg of commercial graphene or CNT powder was dispersed in 10 mL of 0.01 wt% Triton X-100 aqueous solution using ultrasonication for 0.5 h. Then, 0.5 mL of 0.2 wt% N-lauryl acrylate (LA133) aqueous solution, 17 mL of water, and 25 mL of ethanol were added to the graphene or CNT aqueous solution with continuous stirring. A certain volume of as-obtained dispersion was vacuum-filtered using a Celgard 2400 separator as the filter membrane, followed by washing with water. Finally, the product was dried at 60 °C for 6 h.

Preparation of S/CB Cathode: The impregnation of sulfur was carried out by mixing the CB power (Kejing Materials Technology Co., Ltd., China) with sublimed sulfur in a 1:4 weight ratio (respectively). Then, the mixture was heated in a sealed glass bottle at 155 °C for 6 h. In order to prepare the active material slurry, the as-synthesized S/CB composite was mixed with CB, LA133, and isopropanol. The weight ratio of S/CB composite, CB, and LA133 was 8:1:1, respectively. The slurry was further casted onto an Al foil current collector and dried at 60 °C for 6 h in a vacuum oven, which resulted in the formation of S/CB cathode with the sulfur content of 64 wt%. The areal sulfur mass loading of S/CB cathode was controlled to be 3.5 mg cm^{-2}.

Preparation of S/CNT Cathode: First, the commercial CNT powder was dispersed in Triton X-100 aqueous solution, followed by vacuum-filtration through a nylon filter membrane (pore size is 0.45 μm). After washing with water and drying at 60 °C for 1 h, a freestanding CNT paper was peeled from the nylon membrane. In order to prepare the self-supporting cathode, sulfur was added to CS_2, and then, dropped in CNT paper. The weight ratio of sulfur and CNT was controlled to be 7:3, respectively. After drying at room temperature, the S/CNT paper was

transformed into a sealed glass bottle and heated at 155 °C for 6 h. The as-synthesized S/CNT paper was cut into small plates and directly used as the self-supporting cathode. The areal sulfur mass loading of the S/CNT cathode was controlled to be 8.0 mg cm^{-2}.

Electrochemical Measurement: The 2032 coin-type cells were assembled in a glove box, filled with Ar gas (<1 ppm of O_2), and using the S/CB or S/CNT cathodes, Li foil anode, and modified separators. All the cathodes used in this work have areas of about 1.13 cm^2. The electrolyte was bis(trifluoromethane) sulfonamide lithium salt (1 M) in a mixed solvent of 1,2-dimethoxyethane and 1,3-dioxolane (v/v = 1:1) with $LiNO_3$ (2 wt%). The ratios of electrolyte to S for S/CB and S/CNT cathodes were controlled to be 10 and 20 µL mg^{-1}, respectively. It should be pointed out that the addition of $LiNO_3$ is beneficial for the cycling stability of Li–S cells, although the coin cell with $Ni_3(HITP)_2$/PP separator can exhibit improved CE and cycling stability in the absence of $LiNO_3$ when compared with the coin cell with PP separator (Figure S21, Supporting Information). The galvanostatic charge/discharge performance was tested using a LAND CT2001A cell testing system at 25 °C. All of the capacities were calculated according to the mass of sulfur.

Characterization: The XRD patterns were recorded on a Rigaku MiniFlex 600 diffractometer at 30 kV, and Cu-Kα (λ = 1.5418 Å) at ambient temperature. The AFM measurements were performed on an Agilent 5500 with tapping mode. The SEM images were collected on a JSM6700-F at 10 kV. The nitrogen sorption isotherms were measured at liquid nitrogen temperature of 77 K using an automatic volumetric adsorption equipment (Belsorp Max) after degassing it at 100 °C for 12 h. The specific surface area was calculated using the Brunauer–Emmett–Teller model, whereas the pore size distribution was simulated using the nonlocal density functional theory model. The conductivities of $Ni_3(HITP)_2$ membrane and powder pellets were measured at room temperature with a Keithley 4200 SCS semiconductor parameter analyzer. The UV–Vis absorption spectra were obtained using a PE Lambda 950 UV/Vis/NIR.

Supporting Information

Supporting Information is available from the Wiley Online Library or from the author.

Acknowledgements

Y.Z. and F.P. contributed equally to this work. The authors acknowledge the support from National Key R&D Program of China (Grant No. 2017YFA0206802), the MOST of China (Grant No. 2015CB932300), the Strategic Priority Research Program of the Chinese Academy of Sciences (Grant No. XDB20000000), Key Research Program of Frontier Science, CAS (Grant No. QYZDB-SSW-SLH023), the NSFC (Grant No. 21773245, 51402293), the Fundamental Research Funds for the Central Universities (Grant No. 20720160080), Scientific Research and Equipment Development Project of CAS (Grant No. YZ201609), and the NSF of Fujian Province (Grant Nos. 2016J06006 and 2016J05053).

Conflict of Interest

The authors declare no conflict of interest.

Keywords

conductive metal–organic frameworks, crystalline microporous membrane, functional separator, high sulfur loading, Li–S batteries

Received: July 4, 2018
Revised: August 24, 2018
Published online: September 19, 2018

[1] A. Manthiram, Y. Z. Fu, S. H. Chung, C. X. Zu, Y. S. Su, *Chem. Rev.* **2014**, *114*, 11751.
[2] Y. X. Yin, S. Xin, Y. G. Guo, L. J. Wan, *Angew. Chem., Int. Ed.* **2013**, *52*, 13186.
[3] Q. Pang, X. Liang, C. Y. Kwok, L. F. Nazar, *Nat. Energy* **2016**, *1*, 16132.
[4] Y. Yang, G. Y. Zheng, Y. Cui, *Chem. Soc. Rev.* **2013**, *42*, 3018.
[5] X. L. Ji, K. T. Lee, L. F. Nazar, *Nat. Mater.* **2009**, *8*, 500.
[6] Z. W. Seh, W. Y. Li, J. J. Cha, G. Y. Zheng, Y. Yang, M. T. McDowell, P. C. Hsu, Y. Cui, *Nat. Commun.* **2013**, *4*, 1331.
[7] M. Q. Zhao, Q. Zhang, J. Q. Huang, G. L. Tian, J. Q. Nie, H. J. Peng, F. Wei, *Nat. Commun.* **2014**, *5*, 3410.
[8] X. Y. Tao, J. G. Wang, C. Liu, H. T. Wang, H. B. Yao, G. Y. Zheng, Z. W. Seh, Q. X. Cai, W. Y. Li, G. M. Zhou, C. X. Zu, Y. Cui, *Nat. Commun.* **2016**, *7*, 11203.
[9] Z. M. Zheng, H. C. Guo, F. Pei, X. Zhang, X. Y. Chen, X. L. Fang, T. H. Wang, N. F. Zheng, *Adv. Funct. Mater.* **2016**, *26*, 8952.
[10] F. Pei, T. H. An, J. Zang, X. J. Zhao, X. L. Fang, M. S. Zheng, Q. F. Dong, N. F Zheng, *Adv. Energy Mater.* **2016**, *6*, 1502539.
[11] S. Jin, S. Xin, L. J. Wang, Z. Z. Du, L. N. Cao, J. F. Chen, X. H. Kong, M. Gong, J. L. Lu, Y. W. Zhu, H. X. Ji, R. S. Ruoff, *Adv. Mater.* **2016**, *28*, 9094.
[12] H. L. Pan, J. Z. Chen, R. G. Cao, V. J. Murugesan, N. N. Rajput, K. S. Han, K. Persson, L. Estevez, M. H. Engelhard, J. G. Zhang, K. T. Mueller, Y. Cui, Y. Y. Sh, J. Liu, *Nat. Energy* **2017**, *2*, 813.
[13] X. Liu, J. Q. Huang, Q. Zhang, L. Q. Mai, *Adv. Mater.* **2017**, *29*, 1601759.
[14] R. P. Fang, S. Y. Zhao, Z. H. Sun, D. W. Wang, H. M. Cheng, F. Li, *Adv. Mater.* **2017**, *29*, 1606823.
[15] H. J. Peng, J. Q. Huang, X. B. Cheng, Q. Zhang, *Adv. Energy Mater.* **2017**, *7*, 1700260.
[16] Y. S. Su, A. Manthiram, *Nat. Commun.* **2012**, *3*, 1166.
[17] S. H. Chung, A. Manthiram, *Adv. Mater.* **2014**, *26*, 1360.
[18] S. H. Chung, P. Han, R. Singhal, V. Kalra, A. Manthiram, *Adv. Energy Mater.* **2015**, *5*, 1500738.
[19] J. Sun, Y. M. Sun, M. Pasta, G. M. Zhou, Y. Z. Li, W. Liu, F. Xiong, Y. Cui, *Adv. Mater.* **2016**, *28*, 9797.
[20] Z. A. Ghazi, X. He, A. M. Khattak, N. A. Khan, B. Liang, A. Iqbal, J. X. Wang, H. S. Sin, L. S. Li, Z. Y. Tang, *Adv. Mater.* **2017**, *29*, 1606817.
[21] F. Pei, L. L. Lin, A. Fu, S. G. Mo, D. H. Ou, X. L. Fang, N. F. Zheng, *Joule* **2018**, *2*, 323.
[22] O. M. Yaghi, M. O'Keeffe, N. W. Ockwig, H. K. Chae, M. Eddaoudi, J. Kim, *Nature* **2003**, *423*, 705.
[23] S. Kitagawa, R. Kitaura, S. Noro, *Angew. Chem., Int. Ed.* **2004**, *43*, 2334.
[24] S. Sakaida, K. Otsubo, O. Sakata, C. Song, A. Fujiwara, M. Takata, H. Kitagawa, *Nat. Chem.* **2016**, *8*, 377.
[25] X. L. Cui, K. J. Chen, H. B. Xing, Q. W. Yang, R. Krishna, Z. B. Bao, H. Wu, W. Zhou, X. L. Dong, Y. Han, B. Li, Q. L. Ren, M. J. Zaworotko, B. L. Chen, *Science* **2016**, *353*, 141.
[26] F. Yang, G. Xu, Y. B. Dou, B. Wang, H. Zhang, H. Wu, W. Zhou, J. R. Li, B. L. Chen, *Nat. Energy* **2017**, *2*, 877.
[27] I. Stassen, N. Burtch, A. Talin, P. L. Falcaro, M. Allendorfc, R. Ameloot, *Chem. Soc. Rev.* **2017**, *46*, 3185.
[28] K. Shen, L. Zhang, X. D. Chen, L. M. Liu, D. L. Zhang, Y. Han, J. Y. Chen, J. L. Long, R. Luque, Y. W. Li, B. L. Chen, *Science* **2018**, *359*, 206.
[29] S. Y. Bai, X. Z. Liu, K. Zhu, S. C. Wu, H. S. Zhou, *Nat. Energy* **2016**, *1*, 16094.
[30] R. D. Cakan, M. Morcrette, F. Nouar, C. Davoisne, T. Devic, D. Gonbeau, R. Dominko, C. Serre, G. Ferey, J. M. Tarascon, *J. Am. Chem. Soc.* **2011**, *133*, 16154.
[31] J. W. Zhou, R. Li, X. X. Fan, Y. F. Chen, R. D. Han, W. Li, J. Zheng, B. Wang, X. G. Li, *Energy Environ. Sci.* **2014**, *7*, 2715.
[32] J. M. Zheng, J. Tian, D. X. Wu, M. Gu, W. Xu, C. M. Wang, F. Gao, M. H. Engelhard, J. G. Zhang, J. Liu, J. Xiao, *Nano Lett.* **2014**, *14*, 2345.
[33] Y. Y. Mao, G. R. Li, Y. Guo, Z. P. Li, C. D. Liang, X. S. Peng, Z. Lin, *Nat. Commun.* **2017**, *8*, 14628.

[34] D. Zacher, O. Shekhah, C. Wöllb, R. A. Fischer, *Chem. Soc. Rev.* **2009**, *38*, 1418.
[35] T. Kitao, Y. Y. Zhang, S. Kitagawa, B. Wang, T. Uemura, *Chem. Soc. Rev.* **2017**, *46*, 3108.
[36] D. Sheberla, L. Sun, M. A. Blood-Forsythe, S. Er, C. R. Wade, C. K. Brozek, A. A. Guzik, M Dincă, *J. Am. Chem. Soc.* **2015**, *136*, 8859.
[37] L. Sun, M. G. Campbell, M. Dincă, *Angew. Chem., Int. Ed.* **2016**, *55*, 3556.
[38] D. Sheberla, J. C. Bachman, J. S. Elias, C. J. Sun, Y. S. Horn, M Dincă, *Nat. Mater.* **2017**, *16*, 220.
[39] M. S. Yao, W. X. Tang, G. E. Wang, B. Nath, G. Xu, *Adv. Mater.* **2016**, *28*, 5229.
[40] G. D. Wu, J. H. Huang, Y. Zang, J. He, G. Xu, *J. Am. Chem. Soc.* **2017**, *139*, 1360.
[41] W. H. Li, K. Ding, H. R. Tian, M. S. Yao, B. Nath, W. H. Deng, Y. B. Wang, G. Xu, *Adv. Funct. Mater.* **2017**, *27*, 201702067.
[42] T. Zhao, Y. S. Ye, X. Y. Peng, G. Divitini, H. K. Kim, C. Y. Lao, P. R. Coxon, K. Xi, Y. J. Liu, C. Ducati, R. J. Chen, R. V. Kumar, *Adv. Funct. Mater.* **2016**, *26*, 8418.
[43] J. Y. Hwang, H. M. Kim, S. K. Lee, J. H. Lee, A. Abouimrane, M. A. Khaleel, I. Belharouak, A. Manthiram, Y. K. Sun, *Adv. Energy Mater.* **2016**, *6*, 1501480.
[44] Z. B. Xiao, Z. Yang, L. Wang, H. G. Nie, M. E. Zhong, Q. Q. Lai, X. J. Xu, L. J. Zhang, S. M. Huang, *Adv. Mater.* **2015**, *27*, 2891.
[45] H. Q. Wang, W. C. Zhang, H. K. Liu, Z. P. Guo, *Angew. Chem., Int. Ed.* **2016**, *55*, 3992.
[46] G. M. Zhou, E. Paek, A. Manthiram, *Nat. Commun.* **2015**, *6*, 7760.
[47] Z. Li, J. T. Zhang, Y. M. Chen, J. Li, X. W. Lou, *Nat. Commun.* **2015**, *6*, 8850.
[48] W. D. Zhou, B. K. Guo, H. C. Gao, J. B. Goodenough, *Adv. Energy Mater.* **2016**, *6*, 1502059.
[49] S. H. Chung, C. H. Chang, A. Manthiram, *ACS Nano* **2016**, *10*, 10462.
[50] R. P. Fang, S. Y. Zhao, P. X. Hou, M. Cheng, S. G. Wang, H. M. Cheng, C. Liu, F. Li, *Adv. Mater.* **2016**, *28*, 3374.
[51] F. Pei, L. L. Lin, D. H. Ou, Z. M. Zheng, S. G. Mo, X. L. Fang, N. F. Zheng, *Nat. Commun.* **2017**, *8*, 482.
[52] L. Chen, J. Kim, T. Ishizuka, Y. Honsho, A. Saeki, S. Seki, H. Ihee, D. L. Jiang, *J. Am. Chem. Soc.* **2009**, *131*, 7287.